Ab initio many-fermion structure calculations on a quantum computer

Weijie Du[1,2], Yangguang Yang[1], Zixin Liu[1,*] Chao Yang[3], and James P. Vary[2]
[1]*Institute of Modern Physics, Chinese Academy of Sciences, Lanzhou 730000, China*
[2]*Department of Physics and Astronomy, Iowa State University, Ames, Iowa 50010, USA and*
[3]*Applied Mathematics and Computational Research Division, Lawrence Berkeley National Laboratory, Berkeley, California 54720, USA*
(Dated: June 13, 2025)

To overcome the limitations of existing algorithms for solving self-bound quantum many-body problems – such as those encountered in nuclear and particle physics – that access only a restricted subset of energy levels and provide limited structural information, we introduce and demonstrate a novel quantum-classical approach capable of resolving the complete bound-state spectrum. This method also provides the total angular momentum J associated with each eigenstate. Our approach is based on expressing the Hamiltonian in second-quantized form within a novel input model combined with a scan scheme, enabling broad applicability to configuration-interaction calculations across diverse fields. We apply this hybrid method to compute, for the first time, the bound-state spectrum together with corresponding J values of ^{20}O using a realistic strong-interaction Hamiltonian. Our approach applies to hadron spectra and J values solved in the relativistic Basis Light-Front Quantization approach.

arXiv:2505.19906v1 [nucl-th] 26 May 2025

Introduction.– Ab initio, or first principles, Hamiltonian many-body calculations are widely employed in diverse fields such as quantum chemistry [1, 2], nuclear physics [3–6], condensed matter physics [7, 8], and quantum field theories [9, 10]. Classical computing faces the daunting challenge of exponentially increasing resources needed to obtain practical results, for example, to test the underlying interactions or search for novel phenomena. Recent advances in quantum computing have unlocked exciting opportunities for performing efficient first-principles many-body calculations [11–15] but practical algorithms for the full spectra using real-space interactions have yet to emerge. We introduce a general-purpose framework and adopt the self-bound nucleus as an illustrative example to demonstrate how it provides access to the full spectra including determination of the J values with strongly-interacting real-space interactions.

Several quantum algorithms have been adopted to quantum many-body structure calculations, such as the variational quantum eigensolver [13, 14, 16–21], imaginary time quantum eigensolver [22, 23], and quantum subspace expansion methods [24–30]. However, these algorithms primarily target the energies of a limited set of states, mostly the ground state, and struggle to access other structural information essential for understanding a system's response to external probes [31–43], nuclear reactions [44–51], and scattering dynamics [52–61].

Meanwhile, systematically inputting many-fermion Hamiltonians into quantum computers is challenging. Especially, for the Hamiltonians including many-body interactions (e.g., in nuclear and particle physics), the Jordan-Wigner (JW) [62, 63] and Bravyi-Kitaev (BK) [64, 65] schemes become inefficient, as compiling such terms in the Hamiltonian incurs significant overhead and produces extensive Pauli strings. Oracle-based approaches, such as the linear combination of unitaries (LCU) [66, 67], also face growing challenges in designing practical oracles to extract numerous Hamiltonian matrix elements and to uncompute ancilla qubits.

We introduce a new quantum-classical method for *ab inito* structure calculations of many-fermion systems. This approach incorporates a unique two-fold scan scheme that systematically resolves the eigenenergies and corresponding J values of the Hamiltonian eigenstates. For the first time, we compute the full spectrum, along with the corresponding J values, of ^{20}O using quantum algorithms based on a realistic strong-force interaction [68] developed from fundamental theories [69–71]. The same method applies directly to relativistic Hamilonians derived from quantum field theory and expressed in the Basis Light-Front Quantization (BLFQ) framework [72–77].

As a crucial ingredient of this method, we propose a new Hamiltonian input scheme based on a novel circuit representation of the fermion operators that enforces constraints of valid many-body configurations in configuration interaction (CI) calculations. This input scheme eliminates the overhead associated with compiling fermionic operators into Pauli strings that is required by the JW and BK transformations. It is also oracle-free, and there is no need for any uncomputations. Additionally, this input scheme preserves Hamiltonian symmetries, a valuable feature to efficiently pruning Hilbert spaces for tailored eigenvalue calculations.

In the following, we begin with our general discussion of the formalism, Hamiltonian input scheme, and hybrid method. Then, we present the structure calculation of ^{20}O using our method. The proposed method is easily seen to be applicable to CI calculations across various fields.

Formalism.– The Green's function formalism is a forefront research topic in classical computing [78–80] as well as quantum computing [81–87]. We can calculate the retarded Green's function $G(E) = 1/(E - H)$ (referred to

as the resolvent), where it is understood that H includes an infinitesimal imaginary part $H \to H - i\epsilon$ with $\epsilon > 0$, and that $||H||_2 \leq 1$ (one rescales H otherwise). The resolvent can be expressed as [88]:

$$G(E) = -i \int_{-\infty}^{\infty} \exp[iEt] \exp[-iHt]\, dt. \tag{1}$$

We approximate $\exp[-iHt]$ with the Chebyshev polynomial (CP) expansion [89, 90]

$$\exp[-iHt] = \sum_{n=0}^{\infty} (-i)^n (2 - \delta_{n,0}) J_n(t) T_n(H), \tag{2}$$

where $J_n(\cdot)$ is the Bessel function of the first kind and $T_n(\cdot)$ denotes the CP of the first kind [91].

We evaluate the integral using a discrete Fourier transform [88, 91]. With N grid points, the time is given by $t = \pi\tau$ where $\tau = 0, 1, \cdots, N-1$. The discrete energy points are $E_p = 2p/N$, where $p = -N/2, \cdots, N/2$, with N being even. We have

$$\langle \psi_{\rm out}|G(E_p)|\psi_{\rm in}\rangle = -i\pi \Bigg[\sum_{\tau=0}^{N-1} e^{2\pi i p\tau/N} \times \sum_{n=0}^{n_{\max}(\tau)} (-i)^n (2-\delta_{n,0}) J_n(\pi\tau) \langle \psi_{\rm out}|T_n(H)|\psi_{\rm in}\rangle \Bigg]. \tag{3}$$

where $|\psi_{\rm in}\rangle$ and $|\psi_{\rm out}\rangle$ are two many-body states. Here, we truncate the CP expansion (i.e., the second summation) utilizing the asymptotic form of $J_n(\pi\tau)$ and take $n_{\max}(\tau) > e\pi\tau/2 \approx 4\tau$ [88]. The truncation error dramatically decreases with increasing $n_{\max}(\tau)$ [89, 92]. The Chebyshev moment $\langle \psi_{\rm out}|T_n(H)|\psi_{\rm in}\rangle$ captures the many-body nature.

The resolvent has broad applications in solving the structure and dynamics of quantum many-body problems. As a first attempt, we focus on establishing the framework for quantum computing many-fermion structure problems in this work. To date, this has not been discussed in the literature.

Hamiltonian input scheme.– We introduce a novel and efficient *input scheme* for general second-quantized many-fermion Hamiltonian

$$H = \sum_j \langle Q_j|H|P_j\rangle b^\dagger_{Q_j} b_{P_j}. \tag{4}$$

Here, for each *monomial* indexed by $j \in [0, \mathcal{D}-1]$, we denote $Q_j \mapsto \{p_j, q_j, \cdots, r_j\}$ and $P_j \mapsto \{u_j, v_j, \cdots, w_j\}$, where we order the single-particle (SP) bases as $p_j < q_j < \cdots < r_j$ and $u_j < v_j < \cdots < w_j$. The *few-body* matrix element is $\langle Q_j|H|P_j\rangle \equiv \langle p_j, q_j, \cdots, r_j|H|u_j, v_j, \cdots, w_j\rangle$. We also have $b^\dagger_{Q_j} \equiv a^\dagger_{p_j} a^\dagger_{q_j} \cdots a^\dagger_{r_j}$ and $b_{P_j} \equiv a_{w_j} \cdots a_{v_j} a_{u_j}$. Here the fermion operators act on the occupation mode of SP bases as $a^\dagger|0\rangle = |1\rangle$, $a|1\rangle = |0\rangle$, $a^\dagger|1\rangle = a|0\rangle = 0$; and they obey the anticommutation relations $\{a_p, a^\dagger_q\} = \delta_{p,q}$, $\{a_p, a_q\} = \{a^\dagger_p, a^\dagger_q\} = 0$.

This input model is based on the direct basis encoding scheme, which maps $N_{\rm sp}$ SP bases to the qubits in the system register "s". A Fock state is then encoded as $|\mathcal{F}\rangle = |b_0\rangle_0 |b_1\rangle_1 \cdots |b_{N_{\rm sp}-1}\rangle_{N_{\rm sp}-1}$, where each qubit in s corresponds to a specific SP basis, and $|b_p\rangle_p = |0\rangle$ or $|1\rangle$ denotes that the pth basis is vacant or occupied.

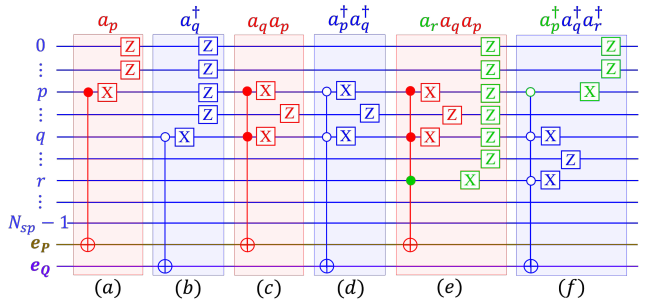

FIG. 1. (color online) From left to right: the circuit representations of a_p, $a^\dagger_q$, $a_q a_p$, and $a^\dagger_p a^\dagger_q$, $a_r a_q a_p$, and $a^\dagger_p a^\dagger_q a^\dagger_r$ (with $p < q < r$). The standard notations of quantum gates [93] are adopted.

We introduce systematic circuit representations for various combinations of fermion operators. These novel representations are reminiscent of Boolean masking [94]. The fermion operators are represented by operations on qubit strings in the system register s that encodes many-fermion states, where corresponding validation information is attached to each processed qubit string to distinguish physical operations from nonphysical ones.

We explain these circuit representations by illustrations in Fig. 1. In addition to the register s, we employ two "*error*" registers, e_P and e_Q (both initialized as $|1\rangle$), to encode the validation information for the actions of annihilation and creation operators, respectively. For example, the circuit for a_p operates as follows: (1) controlled by $|b_p\rangle_p = |1\rangle$, we flip the state $|y\rangle_{e_P} = |1\rangle$ to $|0\rangle$; (2) we then apply a X gate to $|b_p\rangle_p$, aiming to annihilate the occupation; (3) we employ a set of Z gates on qubits with indices ranging from 0 to $p-1$, whereby these Z gates detect the phase factor due to anticommutation relations. To this end, we note that only a valid operation of a_p on $|b_p\rangle_p$ results in the states $|b_p\rangle_p = |0\rangle$ and $|y\rangle_{e_P} = |0\rangle$.

We apply the same idea to design the circuit for $a^\dagger_q$, where, in this case, we flip $|y\rangle_{e_Q} = |1\rangle$ to $|0\rangle$ controlled by $|b_q\rangle_q = |0\rangle$. Only a valid operation results in the states $|b_q\rangle_q = |1\rangle$ and $|y\rangle_{e_Q} = |0\rangle$.

With these elementary circuits, we can construct circuit representations of various combinations of fermion operators, as showcased in Fig. 1(c)-(f). Additional optimizations are also applicable, e.g., cancellations of the

Z gates and simplifications of paired operators such as $a_p^\dagger a_p$.

Our circuit representations of fermion operators are more intuitive and efficient than the JW and BK transformations, particularly in nuclear and particle physics applications where many-body interactions are present. Unlike the JW and BK transformations, which often require compiling each many-body operator into multiple Pauli strings, our design avoids this compilation overhead; this saving also reduces overhead in subsequent Hamiltonian encoding.

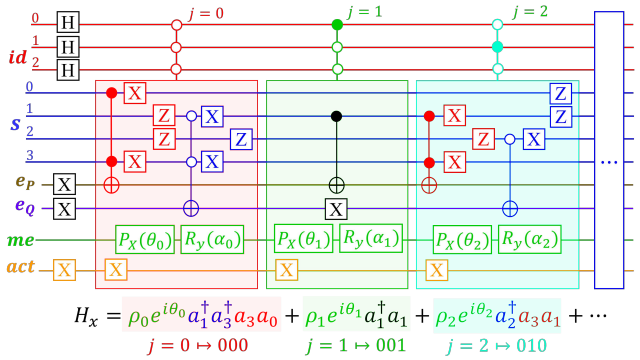

FIG. 2. (color online) Illustration: the circuit of constructing the forward walk state based on the model Hamiltonian H_x. The register s encodes Fock states. The j $(= 0, 1, 2)$ values index the monomials in H_x. Standard notations [93] of elementary quantum gates are adopted except P_X [Eq. (6)].

We can block-encode the second-quantized many-fermion Hamiltonian H utilizing the circuit representations of various combinations of fermion operators. By leveraging the concept of Child's quantum walk [95], we construct the "*forward*" walk state, the many-fermion state $|\mathcal{F}\rangle$, according to H as

$$\mathscr{T}_f |\mathcal{F}\rangle_s \otimes |0\rangle_a = \frac{1}{\sqrt{\mathcal{B}}} \sum_{j=0}^{\mathcal{B}-1} \xi_{\mathcal{F},j} e^{i\beta_j} |j\rangle_{id} |\mathcal{F}_j\rangle_s \times |y^P_{\mathcal{F},j}\rangle_{e_P} |y^Q_{\mathcal{F},j}\rangle_{e_Q} |\rho_j\rangle_{me} |v_j\rangle_{act} , \quad (5)$$

where $\mathscr{T}_f$ defines the operation to construct the walk state [see Supplementary Material (SM) for more details] and "a" denotes all the ancilla registers. For explanatory purposes, we showcase the circuit for the walk-state construction in Fig. 2.

In Eq. (5), we identify each term in the summation with a specific j value in the "index" register id. Indeed, each term tracks the action of the jth monomial $\langle Q_j|H|P_j\rangle b^\dagger_{Q_j} b_{P_j}$ of H on $|\mathcal{F}\rangle$ encoded in the register s, where the auxiliary information is recorded by the ancilla registers. $\xi_{\mathcal{F},j}$ records the actions of the Z gates in our fermionic circuit representations and it takes the values of ± 1. As mentioned above, we record the validation messages of sequential actions of $b^\dagger_{Q_j}$ and b_{P_j} on $|\mathcal{F}\rangle$ by the states $|y^Q_{\mathcal{F},j}\rangle_{e_Q}$ and $|y^P_{\mathcal{F},j}\rangle_{e_P}$, respectively. While $y^Q_{\mathcal{F},j}$ and $y^P_{\mathcal{F},j}$ can be either 0 or 1, it is only when $y^P_{\mathcal{F},j} = y^Q_{\mathcal{F},j} = 0$ that $b^\dagger_{Q_j} b_{P_j} |\mathcal{F}\rangle_s$ is valid and produces a physical many-fermion state $|\mathcal{F}_j\rangle_s$ with the corresponding factor $\xi_{\mathcal{F},j}$.

The matrix-element register "*me*" records the scaled few-body matrix element $\langle Q_j|H|P_j\rangle/\Xi$ by the state $e^{i\beta_j}|\rho_j\rangle_{me}$, with $|\rho_j\rangle \equiv \rho_j |0\rangle + \sqrt{1-\rho_j^2}|1\rangle$ and the *max norm* $\Xi \geq \max_j |\langle Q_j|H|P_j\rangle|$. Here the parameters are $\rho_j = |\langle Q_j|H|P_j\rangle|/\Xi \leq 1$ and $\beta_j = \arg[\langle Q_j|H|P_j\rangle]$. In practice, the state $e^{i\beta_j}|\rho_j\rangle_{me}$ can be prepared by applying the modified phase gate $P_X(\beta_j)$ followed by a $R_y(\alpha_j)$ gate [93] to the register state $|0\rangle_{me}$, with

$$P_X(\beta_j)|0\rangle = e^{i\beta_j}|0\rangle , \; P_X(\beta_j)|1\rangle = |1\rangle , \quad (6)$$

and $\alpha_j = 2\arccos\rho_j$.

The action register "*act*" is introduced in practical calculations. Since we take $\mathcal{B} \geq \mathcal{D}$ in creating the walk state, $|v_j\rangle_{act}$ (initialized as $|1\rangle$) serves to distinguish the *null* terms in the summation where the index j does not correspond to any monomial in H. Those null terms are marked as $v_j = 1$, while we have $v_j = 0$ otherwise.

It is straightforward to construct the "*backward*" walk state with the operation $\mathscr{T}_b$ and the many-fermion state $|\mathcal{G}\rangle$ as

$$\mathscr{T}_b |\mathcal{G}\rangle_s \otimes |0\rangle_a = \frac{1}{\sqrt{\mathcal{B}}} \sum_{k=0}^{\mathcal{B}-1} |k\rangle_{id} |\mathcal{G}\rangle_s |0\rangle_{e_P} |0\rangle_{e_Q} |0\rangle_{me} |0\rangle_{act} . \quad (7)$$

These two walk states block-encode the scaled Hamiltonian $H' \equiv H/(\mathcal{B}\Xi)$ as (proof available in the SM)

$$(\langle\mathcal{G}|_s \otimes \langle 0|_a)\mathscr{T}_b^\dagger \mathscr{T}_f (|\mathcal{F}\rangle_s \otimes |0\rangle_a) = \frac{1}{\mathcal{B}\Xi}\langle\mathcal{G}|H|\mathcal{F}\rangle. \quad (8)$$

There are at most $O(N_{\rm sp}^{2k})$ monomials in a general many-fermion Hamiltonian that includes up to k-body interactions. Our scheme requires $\widetilde{O}(N_{\rm sp}^{2k+1})$ gates to input such a Hamiltonian, which represents the lowest rigorous upper bound on the gate cost for encoding a general k-body Hamiltonian. Further incorporation of symmetry principles can reduce this gate cost.

Compared to the conceptual Hamiltonian input scheme based on Child's quantum walk [95–97] and other input schemes [77, 98, 99], our scheme provides a practical circuit design, avoiding challenging oracle design, ancilla uncomputation, and quantum-classical communication for accessing Hamiltonian elements.

Compared to standard LCU [66, 67], our scheme eliminates the need for the "Prepare oracle", which becomes increasingly difficult to design as matrix elements grow. It admits the max norm Ξ for Hamiltonian scaling, which is smaller than the $\mathbb{L}^1$ norm in LCU [100], making our approach more time-efficient for Hamiltonian simulations.

Utilizing our many-fermion Hamiltonian input scheme, we can block encode $T_n(H')$ following the standard protocol of Ref. [101–103]. The gate cost for encoding $T_n(H')$

is $\widetilde{O}(n \cdot N_{\rm sp}^{2k+1})$. Specific circuit representations of the CPs are also available in the SM.

Hybrid method.– We introduce a novel quantum-classical algorithm for the structure calculations of many-fermion systems such as those arising in nuclear and hadronic physics. This algorithm is capable of computing the full bound spectrum and the J values of the energy eigenstates.

In particular, for our bound-state applications, we adopt the resolvent to compute the *spectral function* $F_\psi(E_p) \equiv \mathfrak{Re}\langle\psi|G(E_p)|\psi\rangle$ with the pivot state $|\psi\rangle$. $F_\psi(E_p)$ connects directly to the strength function [88], and its poles correspond to the eigenenergies.

The algorithmic workflow is sketched in Fig. 3(a). We compute the Chebyshev moments $\{\langle\psi|T_n(H')|\psi\rangle\}$ based on our Hamiltonian input scheme. These moments are input to the classical computer to construct $F_\psi(E_p)$, from which we resolve the spectrum. As our input scheme preserves the symmetry of the Hamiltonian, it enables the so-called "M-scheme" calculations. Namely, if we input the pivot to be of a specific projection M of J, then only states of $J \geq |M|$ emerge in the resultant spectrum.

This algorithm admits a two-fold scan scheme: the cascading-M scan and the resolution scan. With a sufficient resolution scale (set by the number of grid points N), only those energy eigenstates with $J \geq M \geq 1$ appear in the spectrum if we compute using the pivot ψ_M of the projection M. If additional states emerge when computing $F_\psi(E_p)$ with the pivot ψ_{M-1} of the projection $M-1$, the J value of these emerging states are $J = M-1$. Following this idea, if we compute a set of $F_\psi(E_p)$ based on pivots with projections in the range $M \in [M_<, M_>]$ (with $M_> > M_< \geq 0$), we can distinguish those eigenstates with $J = M_> - 1, \cdots, J = M_<$.

Finer resolutions may be needed to distinguish closely spaced states. In this case, we improve the resolution by increasing the number of grid points N, thereby incorporating more Chebyshev moments. In practical calculations, we can start with a moderate N value for a rough scan. Finer scans with larger N values follow if one wants to resolve even more closely spaced energy eigenstates.

We evaluate the total number of Chebyshev moments required to construct $F_\psi(E_p)$ is $O(\mathcal{B}\Xi/\Delta)$, where Δ denotes the spectral gap to be resolved between two neighboring states of interest (in, e.g., a low-lying spectrum).

Realistic calculations.– We apply our hybrid method to compute the structure of ^{20}O with a non-relativistic two-body Hamiltonian in a 3D harmonic oscillator (HO) basis. Had we selected a BLFQ example for a hadron, we would employ a 2D HO basis for the transverse motion in light-front coordinates. In this work, we retain the SP bases in the $0d_{5/2}1s_{1/2}$ shell and exclude those in the $0d_{3/2}$ shell. We implement the realistic nuclear interaction from Ref. [68], where we adopt a basis transformation to obtain the few-body Hamiltonian matrix elements in our SP basis set. A total of 110 matrix elements are retained (see Table S3 in the SM). The same techniques can be applied to no-core shell model [6, 105, 106] calculations in future research.

We evaluate the Chebyshev moments using the IBM Qiskit [107] Statevector simulator in noiseless mode; these moments are cross-checked against corresponding classical calculations. In future applications on real quantum hardware, these moments can be evaluated using standard techniques such as the Hadamard test [93].

We apply our two-fold scan scheme to obtain the J values and eigenenergies of the states utilizing simple single-configuration pivots (note that alternative single-configuration pivots may be needed to unconver missing states; additional comments are available in the SM). By applying the cascading-M scan at a coarse resolution scale [Fig. 3(c) and (e)], we can obtain a rough estimation of the eigenenergies and J values of the states that are well-separated from others. With an improved resolution, more spectral information is resolved [Fig. 3(d) and (f)]. In Fig. 3(f), we note regions (marked in cyan and light pink) where finer resolutions are necessary to resolve states with small spectral gaps. Nevertheless, a coarse resolution scale would be sufficient for the low-lying states with larger spectral gaps.

The excitation spectrum of ^{20}O is presented in Fig. 3(b) with the corresponding J values. Our results from the hybrid method agree with the classical results. We expect better agreement with experiments [104] when the SP states of the $0d_{3/2}$ orbit are included.

Summary.– We propose a novel quantum-classical framework for *ab initio* many-fermion structure calculations. This hybrid method is based on an efficient input scheme for general second-quantized many-fermion Hamiltonians. Using this scheme, we quantum compute the Chebyshev moments and input them into a classical computer to calculate the resolvent, from which we obtain the Hamiltonian spectral function. We introduce a two-fold scan scheme to resolve both the energies and J values of the eigenstates from the spectral function. We apply this hybrid method to compute, for the first time, the structure of ^{20}O based on a realistic strong-interaction Hamiltonian, where we resolve the energies and J values of most eigenstates.

Our approach is directly applicable to hadron spectroscopy [72–77]. We also envision our framework being applicable to CI calculations in fields such as quantum chemistry [13, 14], condensed matter physics [108, 109], and field theories [74, 75, 110, 111]. Our method easily generalizes to evaluate static and reaction observables using the well-known response theory [32, 79, 80]. Further developments aim to improve circuit designs by utilizing, e.g., quantum machine learning [112, 113], for calculations on NISQ hardware [114].

Acknowledgements.– We acknowledge fruitful discussions with Peter Love, Pieter Maris, and Andrey M. Shirokov. This work was supported in part by US

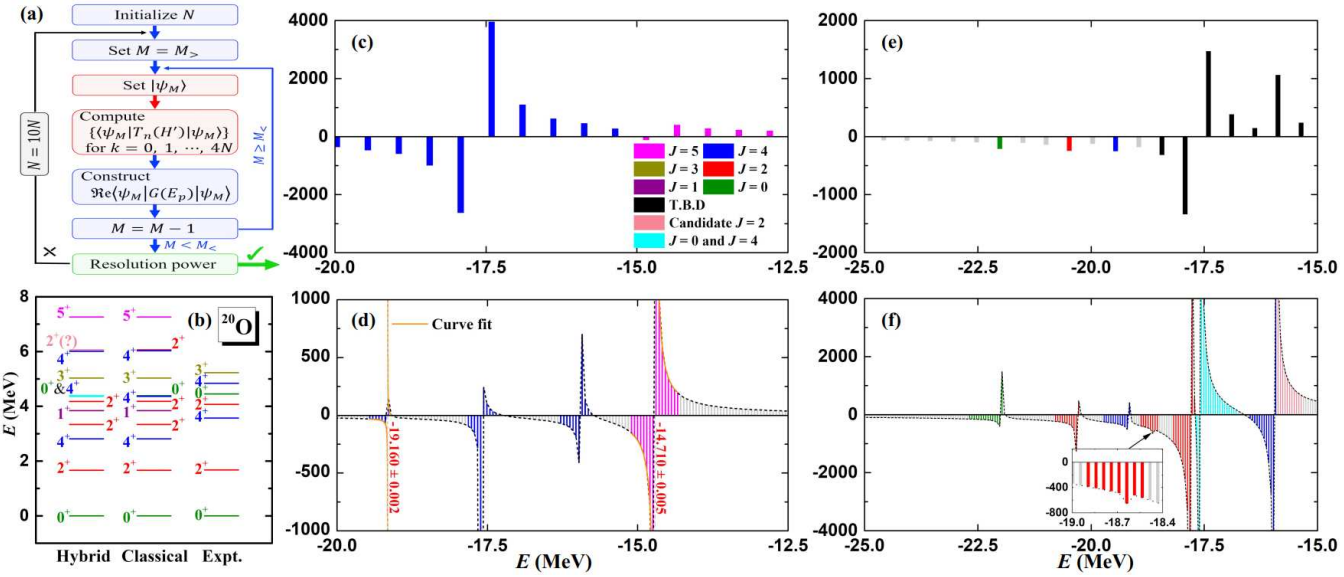

FIG. 3. (color online) **(a)** Algorithmic framework. **(b)** Excitation energies and J values of energy eigenstates of ^{20}O based on the hybrid scheme. These results are compared with classical calculations and experiments [104]. **(c-f)** Spectral functions of ^{20}O as a function of energy E [MeV]. **(c)** and **(d)** are computed with the pivot of the configuration $(1s_{\frac{1}{2},-\frac{1}{2}})(0d_{\frac{5}{2},\frac{1}{2}})(0d_{\frac{5}{2},\frac{3}{2}})(0d_{\frac{5}{2},\frac{5}{2}})$ with $M = 4$. **(e)** and **(f)** are computed with the pivot of the configuration $(1s_{\frac{1}{2},-\frac{1}{2}})(1s_{\frac{1}{2},\frac{1}{2}})(0d_{\frac{5}{2},-\frac{1}{2}})(0d_{\frac{5}{2},\frac{1}{2}})$ with $M = 0$. The number of grid points is $N = 2000$ for **(c)** and **(e)**, while $N = 20000$ for **(d)** and **(f)**. The peaks are fitted according to $f(x) = a_1/(x - E_x + 10^{-6}) + a_2/(x - E_x + 10^{-6})^2 + \eta$ with a_1, a_2, E_x and η being the unknowns [see examples in panel (d)].

DOE Grant DE-SC0023707 under the Office of Nuclear Physics Quantum Horizons program for the "Nuclei and Hadrons with Quantum computers (NuHaQ)" project. This project was also supported in part by NSF Grant No. 2435255 (NQVL-QSTD: Q-BLUE).

* Email: zixinliu@gdlhz.ac.cn

[1] D. Cook, *Handbook of Computational Quantum Chemistry*, Dover Books on Chemistry (Dover Publications, 2012).
[2] B. Bauer, S. Bravyi, M. Motta, and G. K.-L. Chan, Quantum algorithms for quantum chemistry and quantum materials science, Chemical Reviews **120**, 12685 (2020).
[3] E. Caurier, G. Martínez-Pinedo, F. Nowacki, A. Poves, and A. P. Zuker, The shell model as a unified view of nuclear structure, Rev. Mod. Phys. **77**, 427 (2005).
[4] J. Carlson, S. Gandolfi, F. Pederiva, S. C. Pieper, R. Schiavilla, K. E. Schmidt, and R. B. Wiringa, Quantum monte carlo methods for nuclear physics, Rev. Mod. Phys. **87**, 1067 (2015).
[5] M. Hjorth-Jensen, M. P. Lombardo, and U. van Kolck, eds., *An Advanced Course in Computational Nuclear Physics*, Vol. 936 (Springer, 2017).
[6] B. R. Barrett, P. Navratil, and J. P. Vary, Ab initio no core shell model, Prog. Part. Nucl. Phys. **69**, 131 (2013).
[7] E. Fradkin, *Field Theories of Condensed Matter Physics* (Cambridge University Press, 2013).
[8] M. Schreiber and T. Vojta, *Computational Condensed Matter Physics: A Course for Self-Study and the Computer Laboratory*, Advanced Texts in Physics (Springer-Verlag GmbH, 2005).
[9] M. Peskin, *An Introduction To Quantum Field Theory* (CRC Press, 2018).
[10] S. J. Brodsky, H.-C. Pauli, and S. S. Pinsky, Quantum chromodynamics and other field theories on the light cone, Physics Reports **301**, 299 (1998).
[11] R. P. Feynman, Simulating physics with computers, International Journal of Theoretical Physics **21** (1982).
[12] S. Lloyd, Universal quantum simulators, Science **273**, 1073 (1996).
[13] Y. Cao, J. Romero, J. P. Olson, M. Degroote, P. D. Johnson, M. Kieferová, I. D. Kivlichan, T. Menke, B. Peropadre, N. P. D. Sawaya, S. Sim, L. Veis, and A. Aspuru-Guzik, Quantum chemistry in the age of quantum computing, Chemical Reviews **119**, 10856–10915 (2019).
[14] S. McArdle, S. Endo, A. Aspuru-Guzik, S. C. Benjamin, and X. Yuan, Quantum computational chemistry, Reviews of Modern Physics **92**, 10.1103/revmodphys.92.015003 (2020).
[15] T. Albash and D. A. Lidar, Adiabatic quantum computation, Rev. Mod. Phys. **90**, 015002 (2018).
[16] E. F. Dumitrescu, A. J. McCaskey, G. Hagen, G. R. Jansen, T. D. Morris, T. Papenbrock, R. C. Pooser, D. J. Dean, and P. Lougovski, Cloud quantum computing of an atomic nucleus, Phys. Rev. Lett. **120**, 210501 (2018).
[17] J. Tilly, H. Chen, S. Cao, D. Picozzi, K. Setia, Y. Li, E. Grant, L. Wossnig, I. Rungger, G. H. Booth, and J. Tennyson, The variational quantum eigensolver: A review of methods and best practices, Physics Reports

986, 1–128 (2022).
[18] A. M. Romero, J. Engel, H. L. Tang, and S. E. Economou, Solving nuclear structure problems with the adaptive variational quantum algorithm, Physical Review C **105**, 10.1103/physrevc.105.064317 (2022).
[19] C. Sarma, O. Di Matteo, A. Abhishek, and P. C. Srivastava, Prediction of the neutron drip line in oxygen isotopes using quantum computation, Physical Review C **108**, 10.1103/physrevc.108.064305 (2023).
[20] O. Kiss, M. Grossi, P. Lougovski, F. Sanchez, S. Vallecorsa, and T. Papenbrock, Quantum computing of the ^{6}Li nucleus via ordered unitary coupled clusters, Phys. Rev. C **106**, 034325 (2022).
[21] A. Pérez-Obiol, A. M. Romero, J. Menéndez, A. Rios, A. García-Sáez, and B. Juliá-Díaz, Nuclear shell-model simulation in digital quantum computers, Scientific Reports **13**, 10.1038/s41598-023-39263-7 (2023).
[22] M. Motta, C. Sun, A. T. Tan, M. J. O'Rourke, E. Ye, A. J. Minnich, F. G. Brandao, and G. K.-L. Chan, Determining eigenstates and thermal states on a quantum computer using quantum imaginary time evolution, Nature Physics **16**, 205 (2020).
[23] K. Yeter-Aydeniz, R. C. Pooser, and G. Siopsis, Practical quantum computation of chemical and nuclear energy levels using quantum imaginary time evolution and Lanczos algorithms, npj Quantum Inf. **6**, 63 (2020), arXiv:1912.06226 [quant-ph].
[24] C. L. Cortes and S. K. Gray, Quantum krylov subspace algorithms for ground- and excited-state energy estimation, Physical Review A **105**, 10.1103/physreva.105.022417 (2022).
[25] E. N. Epperly, L. Lin, and Y. Nakatsukasa, A theory of quantum subspace diagonalization, SIAM Journal on Matrix Analysis and Applications **43**, 1263–1290 (2022).
[26] W. Kirby, M. Motta, and A. Mezzacapo, Exact and efficient lanczos method on a quantum computer, Quantum **7**, 1018 (2023).
[27] M. Motta, W. Kirby, I. Liepuoniute, K. J. Sung, J. Cohn, A. Mezzacapo, K. Klymko, N. Nguyen, N. Yoshioka, and J. E. Rice, Subspace methods for electronic structure simulations on quantum computers (2023), arXiv:2312.00178 [quant-ph].
[28] N. H. Stair, R. Huang, and F. A. Evangelista, A multireference quantum krylov algorithm for strongly correlated electrons, Journal of Chemical Theory and Computation **16**, 2236 (2020), pMID: 32091895, https://doi.org/10.1021/acs.jctc.9b01125.
[29] W. Du and J. P. Vary, Systematic input scheme for many-boson Hamiltonians with applications to the two-dimensional $\phi 4$ theory, Phys. Rev. D **111**, 016013 (2025), arXiv:2407.13672 [quant-ph].
[30] W. Du and J. P. Vary, Hamiltonian input model and spectroscopy on quantum computers, (2024), arXiv:2402.08969 [quant-ph].
[31] J. Carlson and R. Schiavilla, Euclidean proton response in light nuclei, Phys. Rev. Lett. **68**, 3682 (1992).
[32] J. Carlson, S. Gandolfi, F. Pederiva, S. C. Pieper, R. Schiavilla, K. E. Schmidt, and R. B. Wiringa, Quantum Monte Carlo methods for nuclear physics, Rev. Mod. Phys. **87**, 1067 (2015), arXiv:1412.3081 [nucl-th].
[33] A. Lovato, S. Gandolfi, J. Carlson, S. C. Pieper, and R. Schiavilla, Electromagnetic and neutral-weak response functions of ^{4}He and ^{12}C, Phys. Rev. C **91**, 062501 (2015).
[34] A. Lovato, S. Gandolfi, J. Carlson, S. C. Pieper, and R. Schiavilla, Electromagnetic response of ^{12}C: A first-principles calculation, Phys. Rev. Lett. **117**, 082501 (2016).
[35] S. Bacca, N. Barnea, G. Hagen, M. Miorelli, G. Orlandini, and T. Papenbrock, Giant and pigmy dipole resonances in ^{4}He, ^{16,22}O, and ^{40}Ca from chiral nucleon-nucleon interactions, Phys. Rev. C **90**, 064619 (2014).
[36] J. E. Sobczyk, B. Acharya, S. Bacca, and G. Hagen, Ab initio computation of the longitudinal response function in ^{40}Ca, Phys. Rev. Lett. **127**, 072501 (2021).
[37] J. E. Sobczyk, B. Acharya, S. Bacca, and G. Hagen, ^{40}Ca transverse response function from coupled-cluster theory, Phys. Rev. C **109**, 025502 (2024).
[38] B. Acharya, J. E. Sobczyk, S. Bacca, G. Hagen, and W. Jiang, 16o electroweak response functions from first principles (2024), arXiv:2410.05962 [nucl-th].
[39] J. E. Sobczyk, W. Jiang, and A. Roggero, Spin response of neutron matter in ab initio approach (2024), arXiv:2407.20986 [nucl-th].
[40] V. D. Efros, W. Leidemann, and G. Orlandini, Response functions from integral transforms with a lorentz kernel, Physics Letters B **338**, 130 (1994).
[41] A. Roggero and J. Carlson, Dynamic linear response quantum algorithm, Phys. Rev. C **100**, 034610 (2019), arXiv:1804.01505 [quant-ph].
[42] P. Yin, A. M. Shirokov, H. Li, B. Zhou, X. Zhao, S. Bacca, and J. P. Vary, Alpha-Particle Monopole Form Factors with Ab Initio No-Core Shell Model, (2024), arXiv:2412.18037 [nucl-th].
[43] D. M. Kurkcuoglu, A. Roggero, G. N. Perdue, and R. Gupta, Inference of response functions with the help of machine learning algorithms (2025), arXiv:2501.10583 [quant-ph].
[44] I. Stetcu, Quantum computing for nuclear reactions, EPJ Web Conf. **322**, 03002 (2025).
[45] R. Weiss, A. Baroni, J. Carlson, and I. Stetcu, Solving reaction dynamics with quantum computing algorithms (2025), arXiv:2404.00202 [quant-ph].
[46] V. D. Efros, W. Leidemann, G. Orlandini, and N. Barnea, The lorentz integral transform (lit) method and its applications to perturbation-induced reactions, Journal of Physics G: Nuclear and Particle Physics **34**, R459 (2007).
[47] V. D. Efros, Calculating reactions with use of no-core shell-model states, Phys. Rev. C **99**, 034620 (2019).
[48] M. Goldberger and K. Watson, *Collision Theory*, Dover books on physics (Dover Publications, 2004).
[49] M. Hjorth-Jensen, M. Lombardo, and U. van Kolck, *An Advanced Course in Computational Nuclear Physics: Bridging the Scales from Quarks to Neutron Stars*, Lecture Notes in Physics (Springer International Publishing, 2017).
[50] S. Baroni, P. Navrátil, and S. Quaglioni, Unified ab initio approach to bound and unbound states: No-core shell model with continuum and its application to ^{7}he, Phys. Rev. C **87**, 034326 (2013).
[51] P. Navrátil, S. Quaglioni, I. Stetcu, and B. R. Barrett, Recent developments in no-core shell-model calculations, Journal of Physics G: Nuclear and Particle Physics **36**, 083101 (2009).
[52] T. Luu, M. J. Savage, A. Schwenk, and J. P. Vary, Nucleon-nucleon scattering in a harmonic potential, Phys. Rev. C **82**, 034003 (2010).

[53] W. Du, P. Yin, Y. Li, G. Chen, W. Zuo, X. Zhao, and J. P. Vary, Coulomb excitation of the deuteron in peripheral collisions with a heavy ion, Phys. Rev. C **97**, 064620 (2018), arXiv:1804.01156 [nucl-th].

[54] W. Du, J. P. Vary, X. Zhao, and W. Zuo, Quantum simulation of nuclear inelastic scattering, Phys. Rev. A **104**, 012611 (2021), arXiv:2006.01369 [nucl-th].

[55] S. Sharma, T. Papenbrock, and L. Platter, Scattering phase shifts from a quantum computer, Physical Review C **109**, 10.1103/physrevc.109.l061001 (2024).

[56] P. Wang, W. Du, W. Zuo, and J. P. Vary, Nuclear scattering via quantum computing, Phys. Rev. C **109**, 064623 (2024), arXiv:2401.17138 [nucl-th].

[57] M. A. Sharaf, A. M. Shirokov, W. Du, and J. P. Vary, Applications of the Modified Hulthén-Kohn Method for Bound and Scattering States, (2024), arXiv:2408.05656 [nucl-th].

[58] X. Zhang, Extracting free-space observables from trapped interacting clusters, Phys. Rev. C **101**, 051602 (2020), arXiv:1905.05275 [nucl-th].

[59] X. Zhang, S. R. Stroberg, P. Navrátil, C. Gwak, J. A. Melendez, R. J. Furnstahl, and J. D. Holt, Ab Initio Calculations of Low-Energy Nuclear Scattering Using Confining Potential Traps, Phys. Rev. Lett. **125**, 112503 (2020), arXiv:2004.13575 [nucl-th].

[60] X. Zhang, A non-Hermitian quantum mechanics approach for extracting and emulating continuum physics based on bound-state-like calculations, (2024), arXiv:2408.03309 [nucl-th].

[61] X. Zhang, A non-Hermitian quantum mechanics approach for extracting and emulating continuum physics based on bound-state-like calculations: technical details, (2024), arXiv:2411.06712 [nucl-th].

[62] P. Jordan and E. Wigner, über das paulische äquivalenzverbot, Z. Physik **47** (1928).

[63] M. A. Nielsen, The fermionic canonical commutation relations and the jordan-wigner transform (2005).

[64] S. B. Bravyi and A. Y. Kitaev, Fermionic quantum computation, Annals of Physics **298**, 210–226 (2002).

[65] J. T. Seeley, M. J. Richard, and P. J. Love, The bravyi-kitaev transformation for quantum computation of electronic structure, The Journal of Chemical Physics **137**, 10.1063/1.4768229 (2012).

[66] A. M. Childs and N. Wiebe, Hamiltonian simulation using linear combinations of unitary operations, Quantum Inf. Comput. **12**, 901 (2012).

[67] D. W. Berry, A. M. Childs, R. Cleve, R. Kothari, and R. D. Somma, Simulating hamiltonian dynamics with a truncated taylor series, Phys. Rev. Lett. **114**, 090502 (2015).

[68] I. J. Shin, N. A. Smirnova, A. M. Shirokov, Z. Yang, B. R. Barrett, Z. Li, Y. Kim, P. Maris, and J. P. Vary, Improving the sd-shell effective interaction obtained from the Daejeon16 nucleon-nucleon interaction, Phys. Rev. C **110**, 034306 (2024).

[69] E. Epelbaum, H.-W. Hammer, and U.-G. Meissner, Modern Theory of Nuclear Forces, Rev. Mod. Phys. **81**, 1773 (2009), arXiv:0811.1338 [nucl-th].

[70] E. Epelbaum, H. Krebs, and U. G. Meißner, Improved chiral nucleon-nucleon potential up to next-to-next-to-next-to-leading order, Eur. Phys. J. A **51**, 53 (2015), arXiv:1412.0142 [nucl-th].

[71] E. Epelbaum, H. Krebs, and U. G. Meißner, Precision nucleon-nucleon potential at fifth order in the chiral expansion, Phys. Rev. Lett. **115**, 122301 (2015), arXiv:1412.4623 [nucl-th].

[72] J. P. Vary, H. Honkanen, J. Li, P. Maris, S. J. Brodsky, A. Harindranath, G. F. de Teramond, P. Sternberg, E. G. Ng, and C. Yang, Hamiltonian light-front field theory in a basis function approach, Phys. Rev. C **81**, 035205 (2010), arXiv:0905.1411 [nucl-th].

[73] W. Qian, S. Jia, Y. Li, and J. P. Vary, Light mesons within the basis light-front quantization framework, Phys. Rev. C **102**, 055207 (2020), arXiv:2005.13806 [nucl-th].

[74] M. Kreshchuk, W. M. Kirby, G. Goldstein, H. Beauchemin, and P. J. Love, Quantum simulation of quantum field theory in the light-front formulation, Phys. Rev. A **105**, 032418 (2022), arXiv:2002.04016 [quant-ph].

[75] M. Kreshchuk, S. Jia, W. M. Kirby, G. Goldstein, J. P. Vary, and P. J. Love, Simulating Hadronic Physics on NISQ devices using Basis Light-Front Quantization, Phys. Rev. A **103**, 062601 (2021), arXiv:2011.13443 [quant-ph].

[76] W. Du, Y. Li, X. Zhao, G. A. Miller, and J. P. Vary, Basis Light-Front Quantization for a Chiral Nucleon-Pion Lagrangian, Phys. Rev. C **101**, 035202 (2020), arXiv:1911.10762 [nucl-th].

[77] W. Du and J. P. Vary, Multinucleon structure and dynamics via quantum computing, Phys. Rev. A **108**, 052614 (2023), arXiv:2304.04838 [nucl-th].

[78] J. Schirmer, *Many-Body Methods for Atoms, Molecules and Clusters*, Lecture Notes in Chemistry (Springer International Publishing, 2018).

[79] G. Stefanucci and R. van Leeuwen, *Nonequilibrium Many-Body Theory of Quantum Systems: A Modern Introduction* (Cambridge University Press, 2025).

[80] A. Fetter and J. Walecka, *Quantum Theory of Many-particle Systems*, Dover Books on Physics (Dover Publications, 2003).

[81] E. Kökcü, H. A. Labib, J. K. Freericks, and A. F. Kemper, A linear response framework for quantum simulation of bosonic and fermionic correlation functions, Nature Commun. **15**, 3881 (2024), arXiv:2302.10219 [quant-ph].

[82] P. W. K. Jensen, P. D. Johnson, and A. A. Kunitsa, Near-term quantum algorithm for computing molecular and materials properties based on recursive variational series methods, Physical Review A **108**, 10.1103/physreva.108.022422 (2023).

[83] Y. Tong, D. An, N. Wiebe, and L. Lin, Fast inversion, preconditioned quantum linear system solvers, fast green's-function computation, and fast evaluation of matrix functions, Phys. Rev. A **104**, 032422 (2021).

[84] T. Keen, E. Dumitrescu, and Y. Wang, Quantum algorithms for ground-state preparation and green's function calculation (2021), arXiv:2112.05731 [quant-ph].

[85] F. Libbi, J. Rizzo, F. Tacchino, N. Marzari, and I. Tavernelli, Effective calculation of the green's function in the time domain on near-term quantum processors, Phys. Rev. Res. **4**, 043038 (2022).

[86] R. Sakurai, W. Mizukami, and H. Shinaoka, Hybrid quantum-classical algorithm for computing imaginary-time correlation functions, Phys. Rev. Res. **4**, 023219 (2022).

[87] S. Endo, I. Kurata, and Y. O. Nakagawa, Calculation of the green's function on near-term quantum computers, Phys. Rev. Res. **2**, 033281 (2020).

[88] A. Volya, Time-dependent approach to the continuum shell model, Phys. Rev. C **79**, 044308 (2009).

[89] H. Tal-Ezer and R. Kosloff, An accurate and efficient scheme for propagating the time dependent schrödinger equation, The Journal of Chemical Physics **81**, 3967 (1984), https://pubs.aip.org/aip/jcp/article-pdf/81/9/3967/18950222/3967_1_online.pdf.

[90] A. Weiße, G. Wellein, A. Alvermann, and H. Fehske, The kernel polynomial method, Rev. Mod. Phys. **78**, 275 (2006).

[91] G. Arfken, G. Arfken, H. Weber, and F. Harris, *Mathematical Methods for Physicists: A Comprehensive Guide* (Elsevier Science, 2013).

[92] P. W. K. Jensen, P. D. Johnson, and A. A. Kunitsa, Near-term quantum algorithm for computing molecular and materials properties based on recursive variational series methods, Phys. Rev. A **108**, 022422 (2023).

[93] M. Nielsen and I. Chuang, *Quantum Computation and Quantum Information: 10th Anniversary Edition* (Cambridge University Press, 2010).

[94] T. Helgaker, P. Jorgensen, and J. Olsen, *Molecular Electronic-Structure Theory* (Wiley, 2014).

[95] A. M. Childs, On the relationship between continuous- and discrete-time quantum walk, Communications in Mathematical Physics **294**, 581–603 (2009).

[96] A. M. Childs, Universal computation by quantum walk, Phys. Rev. Lett. **102**, 180501 (2009).

[97] D. W. Berry and A. M. Childs, Black-box hamiltonian simulation and unitary implementation, Quantum Information and Computation **12**, 29 (2012).

[98] D. Liu, W. Du, L. Lin, J. P. Vary, and C. Yang, An Efficient Quantum Circuit for Block Encoding a Pairing Hamiltonian, (2024), arXiv:2402.11205 [nucl-th].

[99] W. A. Simon, C. M. Gustin, K. Serafin, A. Ralli, G. R. Goldstein, and P. J. Love, Ladder operator block-encoding (2025), arXiv:2503.11641 [quant-ph].

[100] R. Babbush, D. W. Berry, I. D. Kivlichan, A. Y. Wei, P. J. Love, and A. Aspuru-Guzik, Exponentially more precise quantum simulation of fermions in second quantization, New Journal of Physics **18**, 033032 (2016).

[101] G. H. Low and I. L. Chuang, Optimal hamiltonian simulation by quantum signal processing, Phys. Rev. Lett. **118**, 010501 (2017).

[102] A. Gilyén, Y. Su, G. H. Low, and N. Wiebe, Quantum singular value transformation and beyond: exponential improvements for quantum matrix arithmetics, in *Proceedings of the 51st Annual ACM SIGACT Symposium on Theory of Computing* (2019) pp. 193–204.

[103] L. Lin, Lecture notes on quantum algorithms for scientific computation (2022), arXiv:2201.08309 [quant-ph].

[104] National nuclear data center, `http://www.nndc.bnl.gov/ensarchivals/`, accessed on 2024-01-23.

[105] P. Navratil, J. P. Vary, and B. R. Barrett, Properties of C-12 in the ab initio nuclear shell model, Phys. Rev. Lett. **84**, 5728 (2000), arXiv:nucl-th/0004058.

[106] P. Navratil, J. P. Vary, and B. R. Barrett, Large basis ab initio no-core shell model and its application to C-12, Phys. Rev. C **62**, 054311 (2000).

[107] Qiskit contributors, Qiskit: An open-source framework for quantum computing (2023).

[108] N. Yoshioka, T. Okubo, Y. Suzuki, Y. Koizumi, and W. Mizukami, Hunting for quantum-classical crossover in condensed matter problems, npj Quantum Inf. **10**, 45 (2024), arXiv:2210.14109 [quant-ph].

[109] Y.-X. Yao, N. Gomes, F. Zhang, C.-Z. Wang, K.-M. Ho, T. Iadecola, and P. P. Orth, Adaptive variational quantum dynamics simulations, PRX Quantum **2**, 030307 (2021).

[110] C. W. Bauer, Z. Davoudi, N. Klco, and M. J. Savage, Quantum simulation of fundamental particles and forces, Nature Rev. Phys. **5**, 420 (2023), arXiv:2404.06298 [hep-ph].

[111] C. W. Bauer, Z. Davoudi, A. B. Balantekin, T. Bhattacharya, M. Carena, W. A. de Jong, P. Draper, A. El-Khadra, N. Gemelke, M. Hanada, D. Kharzeev, H. Lamm, Y.-Y. Li, J. Liu, M. Lukin, Y. Meurice, C. Monroe, B. Nachman, G. Pagano, J. Preskill, E. Rinaldi, A. Roggero, D. I. Santiago, M. J. Savage, I. Siddiqi, G. Siopsis, D. Van Zanten, N. Wiebe, Y. Yamauchi, K. Yeter-Aydeniz, and S. Zorzetti, Quantum simulation for high-energy physics, PRX Quantum **4**, 027001 (2023).

[112] J. Biamonte, P. Wittek, N. Pancotti, P. Rebentrost, N. Wiebe, and S. Lloyd, Quantum machine learning, Nature **549**, 195–202 (2017).

[113] Y. Wang and J. Liu, A comprehensive review of quantum machine learning: from nisq to fault tolerance, Reports on Progress in Physics **87**, 116402 (2024).

[114] J. Preskill, Quantum Computing in the NISQ era and beyond, Quantum **2**, 79 (2018).

[115] J. Suhonen, *From Nucleons to Nucleus: Concepts of Microscopic Nuclear Theory*, Theoretical and Mathematical Physics (Springer Berlin Heidelberg, 2007).

Supplementary Material: Ab initio many-fermion structure calculations on a quantum computer

Weijie Du[1,2], Yangguang Yang[1], Zixin Liu[1,*] Chao Yang[3], and James P. Vary[2]

[1]Institute of Modern Physics, Chinese Academy of Sciences, Lanzhou 730000, China
[2] Department of Physics and Astronomy, Iowa State University, Ames, Iowa 50010, USA
[3]Applied Mathematics and Computational Research Division, Lawrence Berkeley National Laboratory, Berkeley, California 94720, USA

WALK STATES CONSTRUCTION AND HAMILTONIAN INPUT SCHEME

We first construct the *forward* walk state. Provided the Fock state $|\mathcal{F}\rangle$, we prepare the state of multiple quantum registers as

$$|\Phi_0\rangle = |0\rangle_{id}\,|\mathcal{F}\rangle_s\,|1\rangle_{e_P}\,|1\rangle_{e_Q}\,|0\rangle_{me}\,|1\rangle_{act}\,. \tag{9}$$

Here the index register "*id*" is initialized as $|0\rangle$. The qubits in the system register "*s*" encode the Fock state $|\mathcal{F}\rangle$ in terms of the binary string $\{b_0 b_1 \cdots b_{N_{\rm sp}-1}\}$. The single-qubit registers "e_P", "e_Q" and "*act*" are initialized as $|1\rangle$. The single-qubit register "*me*" is initialized as $|0\rangle$. The roles of these registers will be clear in the following text.

We first apply the diffusion operator to *id* register and $|\Phi_0\rangle$ becomes

$$|\Phi_1\rangle = \frac{1}{\sqrt{\mathcal{B}}}\sum_{j=0}^{\mathcal{B}-1}|j\rangle_{id}\,|\mathcal{F}\rangle_s\,|1\rangle_{e_P}\,|1\rangle_{e_Q}\,|0\rangle_{me}\,|1\rangle_{act}\,, \tag{10}$$

where $\mathcal{B}\geq\mathcal{D}$ with $\mathcal{D}$ denoting the total number of monomials in H [Eq. (4) in the main text]. Note that the diffusion operator can produce more j values than the total number of monomials in H. We label each monomial in H with a specific index j. The jth monomial takes the form of $\langle Q_j|H|P_j\rangle b^\dagger_{Q_j} b_{P_j}$. Then, we implement the circuit operations of b_{P_j} and $b^\dagger_{Q_j}$ controlled by j encoded in the index register. With these implementations, we have

$$|j\rangle_{id}\,|\mathcal{F}\rangle_s\,|1\rangle_{e_P}\,|1\rangle_{e_Q}\,|0\rangle_{me}\,|1\rangle_{act}\rightarrow|j\rangle_{id}\,\xi_{\mathcal{F},j}\,|\mathcal{F}_j\rangle_s\,|y^P_{\mathcal{F},j}\rangle_{e_P}\,|y^Q_{\mathcal{F},j}\rangle_{e_Q}\,e^{i\beta_j}\,|\rho_j\rangle_{me}\,|0\rangle_{act}\,, \tag{11}$$

where we have $\xi_{\mathcal{F},j}\,|\mathcal{F}_j\rangle_s = b^\dagger_{Q_j} b_{P_j}\,|\mathcal{F}\rangle_s$. The factor $\xi_{\mathcal{F},j}$ takes the value of ±1, which is obtained from the sequences of Pauli-Z gates in the circuit representation of the fermion operators acting on respective sequences of qubits that encode the occupation status of relevant SP bases. $|\mathcal{F}_j\rangle_s$ is a binary string. While $b^\dagger_{Q_j} b_{P_j}\,|\mathcal{F}\rangle_s$ should be understood formally, their circuit execution may produce binary strings $|\mathcal{F}_j\rangle_s$ that is nonphysical. As mentioned above, we record the validation message of the sequential actions of $b^\dagger_{Q_j}$ and b_{P_j} on $|\mathcal{F}\rangle$ by the states $|y^Q_{\mathcal{F},j}\rangle_{e_Q}$ and $|y^P_{\mathcal{F},j}\rangle_{e_P}$, respectively. While both $y^Q_{\mathcal{F},j}$ and $y^P_{\mathcal{F},j}$ can take the value of 0 or 1, it is only when $y^P_{\mathcal{F},j}=y^Q_{\mathcal{F},j}=0$ that $b^\dagger_{Q_j} b_{P_j}\,|\mathcal{F}\rangle_s$ produces a physical many-fermion state $|\mathcal{F}_j\rangle_s$ with the corresponding phase factor $\xi_{\mathcal{F},j}$.

We operate on the single-qubit register *me* in Eq. (11) according to the scaled *few-body* matrix element $\langle Q_j|H|P_j\rangle/\Xi$ with $\Xi\geq\max_j|\langle Q_j|H|P_j\rangle|$. The operation is

$$|0\rangle_{me}\rightarrow e^{i\beta_j}\,|\rho_j\rangle_{me}\,, \tag{12}$$

where $|\rho_j\rangle\equiv\rho_j\,|0\rangle+\sqrt{1-\rho_j^2}\,|1\rangle$. The parameters ρ_j and β_j are determined as

$$\rho_j e^{i\beta_j} = \langle Q_j|H|P_j\rangle/\Xi, \tag{13}$$

where $\rho_j=|\langle Q_j|H|P_j\rangle|/\Xi\leq1$ with and $\beta_j=\arg[\langle Q_j|H|P_j\rangle]$. The operation [Eq. (12)] can be achieved by applying the gate $P_X(\beta_j)$ and sequentially by a $R_y(\alpha_j)$ gate [93] to the register *me*, where

$$P_X(\beta_j)\,|0\rangle = e^{i\beta_j}\,|0\rangle\,,\;P_X(\beta_j)\,|1\rangle=|1\rangle\,,\;\alpha_j=2\arccos\rho_j. \tag{14}$$

* zixinliu@gdlhz.ac.cn

In Eq. (11), we also flip the register state $|1\rangle_{act}$ to $|0\rangle_{act}$ by a Pauli-X gate as the j value indeed corresponds to a monomial.

Following the operations illustrated by Eq. (11), we have the forward walk state

$$|\Phi_2\rangle = \frac{1}{\sqrt{\mathcal{B}}} \sum_{j=0}^{\mathcal{B}-1} \xi_{\mathcal{F},j} e^{i\beta_j} |j\rangle_{id} |\mathcal{F}_j\rangle_s |y^P_{\mathcal{F},j}\rangle_{e_P} |y^Q_{\mathcal{F},j}\rangle_{e_Q} |\rho_j\rangle_{me} |v_j\rangle_{act} . \tag{15}$$

Here we denote the state of act as $|v_j\rangle_{act}$ with $v_j = 0$ or 1. The state $|v_j\rangle_{act}$ helps to distinguish the true contribution from the Hamiltonian monomials to the Fock state $|\mathcal{F}\rangle$, noticing that more j values can be produced by the diffusion operator than the number of Hamiltonian monomials in practical calculations (recall we have $\mathcal{B} \geq \mathcal{D}$). If the j value does correspond to a specific Hamiltonian monomial, we have $v_j = 0$, and v_j is 1 otherwise. In Fig. 2, we present an illustration of constructing the forward walk state based on a model Hamiltonian.

The *backward* walk state $|\Psi_1\rangle$ is prepared as follows. Starting from the Fock state $|\mathcal{G}\rangle$, we initialize the multi-register state

$$|\Psi_0\rangle = |0\rangle_{id} |\mathcal{G}\rangle_s |0\rangle_{e_P} |0\rangle_{e_Q} |0\rangle_{me} |0\rangle_{act} , \tag{16}$$

where the registers e_P, e_Q, me, and act are all initialized as $|0\rangle$, which is to be compared with the initialization of $|\Phi_0\rangle$. We then apply the diffusion operator to the register id, and $|\Psi_0\rangle$ becomes

$$|\Psi_1\rangle = \frac{1}{\sqrt{\mathcal{B}}} \sum_{k=0}^{\mathcal{B}-1} |k\rangle_{id} |\mathcal{G}\rangle_s |0\rangle_{e_P} |0\rangle_{e_Q} |0\rangle_{me} |0\rangle_{act} . \tag{17}$$

The forward and backward walk states block encode the Hamiltonian of the many-fermion system. Indeed, their inner product is

$$\langle\Psi_1|\Phi_2\rangle = \frac{1}{\mathcal{B}} \sum_{j=0}^{\mathcal{B}} \sum_{k=0}^{\mathcal{B}} \xi_{\mathcal{F},j} e^{i\beta_j} \langle k|j\rangle_{id} \langle\mathcal{G}|\mathcal{F}_j\rangle_s \langle 0|y^P_{\mathcal{F},j}\rangle_{e_P} \langle 0|y^Q_{\mathcal{F},j}\rangle_{e_Q} \langle 0|\rho_j\rangle_{me} \langle 0|v_j\rangle_{act} \tag{18}$$

$$= \frac{1}{\mathcal{B}} \sum_{j=0}^{\mathcal{B}} \xi_{\mathcal{F},j} e^{i\beta_j} \langle\mathcal{G}|\mathcal{F}_j\rangle_s \langle 0|y^P_{\mathcal{F},j}\rangle_{e_P} \langle 0|y^Q_{\mathcal{F},j}\rangle_{e_Q} \langle 0|\rho_j\rangle_{me} \langle 0|v_j\rangle_{act}, \tag{19}$$

which correctly produces the many-fermion matrix element of the scaled Hamiltonian $H' = H/(\mathcal{B}\Xi)$ based on the Fock states $|\mathcal{F}\rangle$ and $|\mathcal{G}\rangle$ as well as scaled few-body matrix elements $\{\rho_j e^{i\beta_j}\}$ [Eq. (13)].

We can present $\langle\Psi_1|\Phi_2\rangle$ in terms of the standard form of Hamiltonian block encoding. In particular, we can write the walks states based on the isometries $\mathscr{T}_f$ and $\mathscr{T}_b$ as

$$|\Phi_2\rangle = \mathscr{T}_f |\mathcal{F}\rangle_s \otimes |0\rangle_a , \ |\Psi_1\rangle = \mathscr{T}_b |\mathcal{G}\rangle_s \otimes |0\rangle_a . \tag{20}$$

Here, the ancilla registers are denoted as "a", which include all the registers except the system register s. Then, the Hamiltonian block encoding scheme can be presented as

$$(\langle\mathcal{G}|_s \otimes \langle 0|_a) \mathscr{T}_b^\dagger \mathscr{T}_f (|\mathcal{F}\rangle_s \otimes |0\rangle_a) = \frac{1}{\mathcal{B}\Xi} \langle\mathcal{G}|H|\mathcal{F}\rangle. \tag{21}$$

A few comments on the above Hamiltonian input scheme are as follows. This scheme is non-Hermitian, i.e., $\mathscr{T}_b^\dagger \mathscr{T}_f \neq (\mathscr{T}_b^\dagger \mathscr{T}_f)^\dagger$. While the standard quantum-walk-based input scheme, designed according to Childs' quantum walk, operates in the first-quantization framework and accesses Hamiltonian matrix elements through communication with a precomputed classical database based on row and column indices [95–97], our input scheme works in the second-quantization framework, dynamically computing many-body matrix elements of the scaled Hamiltonian using Fock states, without requiring data exchange with a precomputed classical database.

Meanwhile, our block encoding scheme eliminates the need for uncomputation, which can be costly in typical quantum algorithms [95–97]. Additionally, while the standard walk-state-based input scheme cannot provide a practical circuit design for general Hamiltonians due to challenges in quantum-classical communication, our scheme offers a viable circuit design.

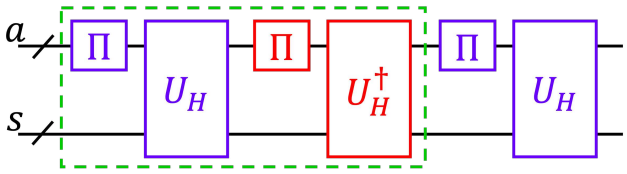

FIG. S1. (color online) Illustration: Circuit for inputting $T_3(H')$ (figure adapted from [29]). Here, s and a denote the system register and the ancilla register, respectively. The slashed line denotes a register that may contain multiple qubits. The circuit enclosed by the dashed green box block-encodes $T_2(H')$.

CIRCUIT REPRESENTATION OF THE CHEBYSHEV POLYNOMIALS

With the Hamiltonian input scheme [Eq. (21)], we can input the Chebyshev polynomials of the first kind [29, 30, 103] as

$$\langle\mathcal{G}|T_{2k+1}(H')|\mathcal{F}\rangle = (\langle\mathcal{G}|_s \otimes \langle 0|_a)\left[U_H\Pi\left(U_H^\dagger\Pi U_H\Pi\right)^k\right]\left(|\mathcal{F}\rangle_s \otimes |0\rangle_a\right), \tag{22}$$

$$\langle\mathcal{G}|T_{2k}(H')|\mathcal{F}\rangle = (\langle\mathcal{G}|_s \otimes \langle 0|_a)\left(U_H^\dagger\Pi U_H\Pi\right)^k\left(|\mathcal{F}\rangle_s \otimes |0\rangle_a\right), \tag{23}$$

with $k = 0,\ 1,\ 2, \cdots$. Here, the reflection operator $\Pi \equiv (2\,|0\rangle_a\,\langle 0|_a - \mathbb{I}_a) \otimes \mathbb{I}_s$ produces the reflection around $|0\rangle_a$ in the auxiliary space. We also define $U_H \equiv \mathscr{T}_b^\dagger \mathscr{T}_f$. Therefore, the quantum circuit for inputting $T_n(H')$ is achieved by alternating applications of the building blocks $U_H\Pi$ and $U_H^\dagger\Pi$ [103], as illustrated in Fig. S1.

REALISTIC HAMILTONIAN FOR THE NUCLEAR MANY-BODY CALCULATION

We compute the eigenenergies and the corresponding total angular momenta of the eigenstates of ^{20}O in this work. We adopt a subspace of the *sd*-valence shell. In particular, we retain the single-particle (SP) basis states in the $0d_{5/2}1s_{1/2}$ orbits, where we exclude those SP bases in the $0d_{3/2}$ orbit. The adopted SP bases are listed in Table S1.

TABLE S1. The SP bases in the $0d_{5/2}1s_{1/2}$ valence shell. The quantum numbers of each SP state are presented, whereas the spin and isospin of the neutrons are understood to be 1/2, while the isospin projection is $-1/2$. Each SP basis is indexed and mapped to a specific qubit.

	SP basis (qubit)	n	l	$2j$	$2m$
$1s_{1/2}$	0	1	0	1	-1
	1	1	0	1	$+1$
$0d_{5/2}$	2	0	2	5	-5
	3	0	2	5	-3
	4	0	2	5	-1
	5	0	2	5	$+1$
	6	0	2	5	$+3$
	7	0	2	5	$+5$

The Hamiltonian of the many-neutron system is

$$H = E_{\text{core}} + \sum_{i=0}^{7}\varepsilon_i a_i^\dagger a_i + \sum_{p<q}^{7}\sum_{r<s}^{7}\langle pq|V|rs\rangle a_p^\dagger a_q^\dagger a_s a_r, \tag{24}$$

where we adopt the phenomenologically successful choices of Ref. [68] and set the SP energy $\varepsilon_i = -3.2079$ MeV for $i = 0, 1$ and $\varepsilon_i = -3.9257$ MeV for $i \in [2, 7]$. We set the core energy to be $E_{\text{core}} = 0$ for computing the excitation spectrum in our work. The two-body interaction matrix elements are derived from the effective *sd*-shell NN interaction [68]. In Table S2, we list these interaction matrix elements in the coupled-JT basis.

We can implement Eq. (8.24) in Ref. [115] to transform the interaction matrix elements from the coupled-JT basis to the elected SP basis. These transformed two-body interaction matrix elements are listed in Table S3 (with indices

TABLE S2. Effective *sd*-shell NN interaction matrix elements in the coupled JT-basis.These elements are quoted from Table S1 in Ref. [68] with $J = 0,\ 1,\ 2,\ 3,\ 4$ and the isospin $T = 1$.

$2j_a$	$2j_b$	$2j_c$	$2j_d$	J	T	V
1	1	1	1	0	1	-1.910
1	1	5	5	0	1	-1.564
5	5	5	5	0	1	-2.439
1	5	1	5	2	1	-1.032
1	5	5	5	2	1	-0.544
5	5	5	5	2	1	-1.119
1	5	1	5	3	1	0.751
5	5	5	5	4	1	-0.152

from 8 to 109). It is noteworthy that an additional factor $(18/A)^{1/3}$ (with $A = 20$) is necessary to scale the interaction matrix elements provided in Table S3 for computing the spectrum of ^{20}O. Indeed, these interaction matrix elements are also applicable to the spectral calculations of additional Oxygen isotopes using the corresponding scaling.

PIVOT CHOICES

Our results in this work are obtained using single-configuration pivots. While a single-configuration pivot is easy to prepare within our hybrid scheme, some states may be absent from the resultant spectral function [e.g., the odd-J states in Fig. 3(f) in the main text]. To uncover these missing odd-J states, we can use an alternative single-configuration pivot. More generally, we can prepare a superposition of simple pivots, e.g., by a linear combination of states [103], to resolve all the eigenstates simultaneously.

TABLE S3. The matrix elements in the SP basis. The indices p, q, r, and s label the SP bases listed in Table S1. The first 8 entries are the SP energies [68]. The rest entries (with index from 8 to 109) are the two-body interaction matrix elements in the SP basis.

index	p	q	r	s	$\langle pq\|H\|rs\rangle$	index	p	q	r	s	$\langle pq\|H\|rs\rangle$	index	p	q	r	s	$\langle pq\|H\|rs\rangle$
0	0	–	0	–	−3.2079	37	4	5	7	2	−0.30186	74	6	7	7	6	−0.15200
1	1	–	1	–	−3.2079	38	4	5	6	3	0.85443	75	0	4	4	0	0.15667
2	2	–	2	–	−3.9257	39	4	5	5	4	−1.28270	76	0	4	3	1	0.84051
3	3	–	3	–	−3.9257	40	0	6	6	0	−0.43767	77	0	4	6	2	−0.26545
4	4	–	4	–	−3.9257	41	0	6	5	1	0.84051	78	0	4	5	3	0.16788
5	5	–	5	–	−3.9257	42	0	6	7	3	−0.37540	79	1	3	4	0	0.84051
6	6	–	6	–	−3.9257	43	0	6	6	4	0.23742	80	1	3	3	1	−0.43767
7	7	–	7	–	−3.9257	44	1	5	6	0	0.84051	81	1	3	6	2	0.37540
8	0	1	1	0	−1.9100	45	1	5	5	1	0.15667	82	1	3	5	3	−0.23742
9	0	1	7	2	−0.90298	46	1	5	7	3	0.26545	83	2	6	4	0	−0.26545
10	0	1	6	3	0.90298	47	1	5	6	4	−0.16788	84	2	6	3	1	0.37540
11	0	1	5	4	−0.90298	48	3	7	6	0	−0.37540	85	2	6	6	2	−0.84271
12	0	5	5	0	−0.14050	49	3	7	5	1	0.26545	86	2	6	5	3	0.43685
13	0	5	4	1	0.89150	50	3	7	7	3	−0.84271	87	3	5	4	0	0.16788
14	0	5	7	2	−0.29678	51	3	7	6	4	0.43685	88	3	5	3	1	−0.23742
15	0	5	6	3	−0.05936	52	4	6	6	0	0.23742	89	3	5	6	2	0.43685
16	0	5	5	4	0.23742	53	4	6	5	1	−0.16788	90	3	5	5	3	−0.42829
17	1	4	5	0	0.89150	54	4	6	7	3	0.43685	91	0	3	3	0	0.45383
18	1	4	4	1	−0.14050	55	4	6	6	4	−0.42829	92	0	3	2	1	0.66449
19	1	4	7	2	0.29678	56	0	7	7	0	−0.73483	93	0	3	5	2	−0.13272
20	1	4	6	3	0.05936	57	0	7	6	1	0.66449	94	0	3	4	3	0.17807
21	1	4	5	4	−0.23742	58	0	7	7	4	−0.29678	95	1	2	3	0	0.66449
22	2	7	1	0	−0.90298	59	0	7	6	5	0.39817	96	1	2	2	1	−0.73483
23	2	7	5	0	−0.29678	60	1	6	7	0	0.66449	97	1	2	5	2	0.29678
24	2	7	4	1	0.29678	61	1	6	6	1	0.45383	98	1	2	4	3	−0.39817
25	2	7	7	2	−1.48990	62	1	6	7	4	0.13272	99	2	5	3	0	−0.13272
26	2	7	6	3	0.64721	63	1	6	6	5	−0.17807	100	2	5	2	1	0.29678
27	2	7	5	4	−0.30186	64	4	7	7	0	−0.29678	101	2	5	5	2	−0.49736
28	3	6	1	0	0.90298	65	4	7	6	1	0.13272	102	2	5	4	3	0.46335
29	3	6	5	0	−0.05936	66	4	7	7	4	−0.49736	103	3	4	3	0	0.17807
30	3	6	4	1	0.05936	67	4	7	6	5	0.46335	104	3	4	2	1	−0.39817
31	3	6	7	2	0.64721	68	5	6	7	0	0.39817	105	3	4	5	2	0.46335
32	3	6	6	3	−0.93736	69	5	6	6	1	−0.17807	106	3	4	4	3	−0.77364
33	3	6	5	4	0.85443	70	5	6	7	4	0.46335	107	0	2	2	0	0.75100
34	4	5	1	0	−0.90298	71	5	6	6	5	−0.77364	108	2	4	4	2	−0.15200
35	4	5	5	0	0.23742	72	1	7	7	1	0.75100	109	2	3	3	2	−0.15200
36	4	5	4	1	−0.23742	73	5	7	7	5	−0.15200	–	–	–	–	–	–